Modelling Tomographic Reconstruction using Scintillator Fibres for active proton imaging

Contact: `adam.illoul@stfc.ac.uk`

A.R.L Illoul
School of Physics,
University of Bristol,
BS8 1TH, United Kingdom

C.D. Armstrong
Deparment of Plasma Physics,
Central Laser Facility, RAL
OX11 0QZ, United Kingdom

1   Abstract

High repetition rate laser facilities require active diagnostic systems in order to process data promptly. Current methods to image the spectral-spatial distribution of protons are incapable of this, and so novel diagnostic tools need to be developed. Here we present software as a proof-of-concept active proton imaging system capable of measuring the spectral-spatial distribution of proton beams. This novel approach utilises tomographic reconstruction, with scintillating fibres as the medium of signal transport. We exhibit the reconstructed images as further projected angles are used, and demonstrate the necessity of correcting for light absorption within a scintillator fibre. We analytically present how the spectral resolution of such a diagnostic tool would vary as further projected angles are used.

2   Introduction

Laser-plasma interactions can be used as prompt, high repetition radiation sources [1]. Characterisation of this radiation is necessary for diagnosing the interactions. One diagnostic tool currently used to observe the highly energetic proton beam from such interactions is Radiochromic Film (RCF) stacks [2]. This diagnostic is capable of separating the proton beam into energy bins and exhibiting the cross-section of the beam at each given energy. These measurements constitute the spectral-spatial distribution of the proton beam.

This diagnostic has only single-shot capabilities, and is impractical for high repetition rate facilities. It is therefore of interest to investigate alternative methods of observing the spectral-spatial distribution of these highly energetic protons. Previous investigations have demonstrated that scintillators can replace RCF stacks using scintillators of unique emissions [3], or scintillators displaced angularly in an "accordion" setup [4], however both techniques are unable to image a wide range of proton energies from a single shot.

A new proposal using scintillators would replace RCF stacks, employing scintillating fibres to tomographically reconstruct the image. This would exploit the technique of resolving spectrally in much the same way that RCF stacks do, but involve lateral signal detection, and computer tomography to reconstruct the proton beam. The scintillating fibres would constitute a fibre mesh of a similar size to RCF, and by adding fibre meshes of a different orientation, a more resolved image could be reconstructed.

This report demonstrates a proof-of-concept reconstruction model, implementing the physical fibres across a pixel grid, and the attenuation of optical light as it travels through the scintillating fibre. The reconstructed image is compared to the original for several mesh arrays oriented uniquely, and its effect on the spectral resolution of the arrangement is discussed.

3   Theory

As highly energetic ionising protons traverse a material they deposit energy. This energy deposition is not uniform, but varies with depth, exhibiting a peak at the end of the protons journey. The entire trend of proton energy deposition to depth is known as the Bragg curve, with the peak named the Bragg peak. Protons with a higher energy will have a Bragg peak that is deeper into a material.

Layers of RCF are used for radiation diagnostics; acting as layers inside such a material, each layer absorbing the Bragg peak dose of a given proton energy. As of such, each layer can distinguish between protons of certain energies. It cannot absorb protons of a unique energy, as it would have to be extremely thin to do so. Instead, each layer absorbs a spectrum of proton energies. The range of this spectrum is known as the spectral resolution of the diagnostic tool. A schematic of this is shown in Fig.1.

This feature is not intrinsic to RCF, but is apparent through all mediums. If layers of scintillator blocks replaced the layers of RCF, then the schematic above still applies. Using scintillator blocks would require the light response to be viewed laterally with a photo-detector. Spectroscopic analysis has been done using this setup for X-rays [5]. However all spatial information is lost within the block of scintillator due to internal diffuse reflections of photons.

This new proposal would instead use a fibre array mesh in place of the scintillator block. With a single proton absorbed by a fibre mesh, the point of interac-
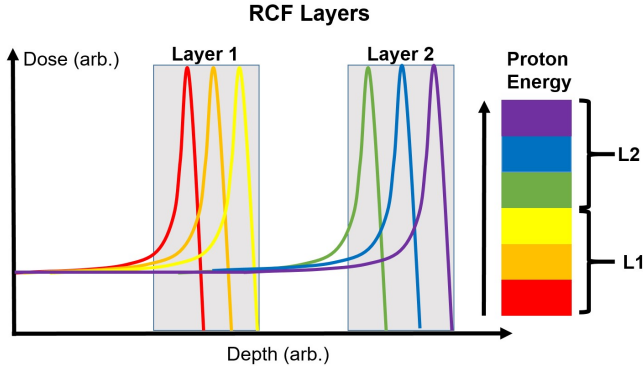
RCF Layers

Figure 1: Schematic of proton energy deposition as a function of depth when interacting with layers of RCF. Layers that are deeper into the diagnostic will absorb protons of higher energies. Each layer will also absorb a distribution of energies, the width of which represents the spectral resolution of each layer, and this is shown as L1 and L2 on the right.
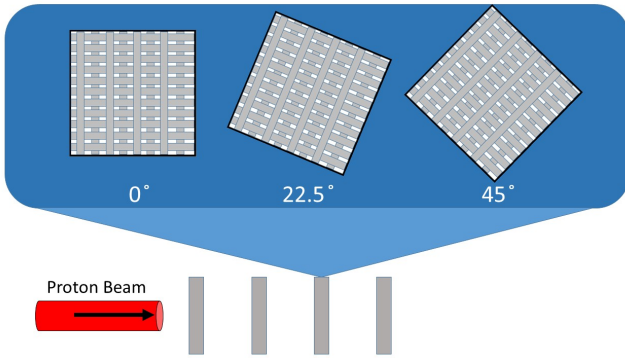
Figure 2: Schematic of the proposed diagnostic. The incident proton beam travels through each layer depositing energy. At each layer, several meshes are packed together, each oriented at a different angle.

tion could be determined through measuring the signal of each fibre end. The spatial resolution of this measurement would be limited by the thickness of the fibre. For a larger complex shape incident on the mesh, such as a circular proton beam, fibre meshes oriented at different angles could be introduced to improve the spatial resolution of such a diagnostic. This introduction of further meshes poses a problem, as the addition of meshes would necessitate a thicker layer. This would cause each layer to absorb a wider spectral range of protons, and thus deplete the spectral resolution. A schematic of the proposed diagnostic is shown in Fig.2.

4   Method

The reconstruction technique utilised the Maximum-Likelihood Expectation Maximisation algorithm [6]. This method iteratively modifies a 'guess' image pixel by pixel by comparing the lateral readouts between the 'guess' image and the measured data. Given an adequate number of measurements from different angles, the reconstructed image will approach that of the original. This method was preferred to Filtered Back Projection (FBP), a commonly used reconstruction algorithm, due to its superiority in reconstruction from few-angle projections [7] [8].

The MLEM algorithm begins with acquiring a prior image that has similar characteristics to the true image, and forward projects this image from each angle used in the original data collection. This forward projection compresses the 'guess' image into the same data format as the measured readout. The algorithm iterates through each pixel and locates the readout values that corresponds to that pixel for both the 'guess' image and the measured image. It then uses a weighting algorithm involving this list of readout values, and returns a ratio that the 'guess' image pixel will be multiplied by. It does this for each pixel within the image. After the last pixel has been modified, the new image is then forward projected again, returning a new list of readouts, and the process continues.

Because the maximum capabilities of this algorithm wanted to be tested, the reconstructed images used were those with the lowest mean standard error (MSE) between itself and the original image. In a laboratory setting this true image is not known, and therefore the reconstructed image with the lowest MSE between itself and the original is unknown. The intended image to reconstruct was chosen as the Shepp-Logan phantom [9] as it is a standard for simulating tomographic reconstructions [10].

To apply the characteristics of light transport within a scintillator, a Monte Carlo simulation was employed to approximate the reduction in signal amplitude as a function of depth in the scintillator fibre. The simulation was provided with the attributes of a scintillating fibre, and the fibres diffuse reflective surface was given a reflectance coefficient of 0.999. This amplitude reduction was applied to the reconstruction process where the signal of a given pixel was reduced depending on its distance from the detector.

The reconstruction technique relied on weighting pixel values in a two dimensional array to be represented in the readout. Using solid fibres, a single pixel may represent more than one physical fibre, and therefore presents a challenge as to how to accurately represent the signal in the readout. This was resolved by writing a separate Python script that calculated the ratios of each solid fibres surface area within a pixel to the pixel itself. The readout signal in the reconstruction method were then weighted by this ratio.

Using the readout from the measured data, we are able to construct the prior image in order to begin the reconstruction technique. This prior image was the back projection of the measured readout. The angles between each simulated mesh (panel) were linearly spaced over 90°. We observed the change in the MSE for each iterated reconstruction, and how the number of panels
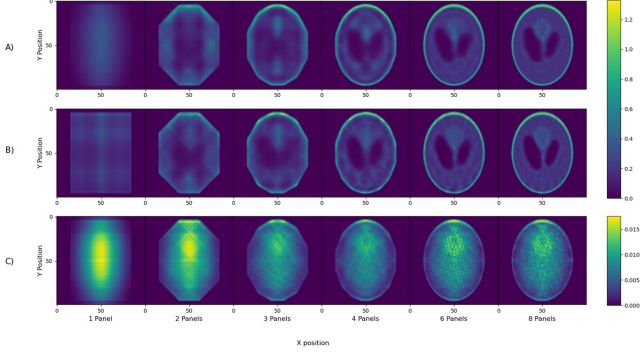
Figure 3: The reconstructed images of the Shepp-Logan phantom using one of three methods. A) is where the measured signal is attenuated, and the reconstruction software accounts for. In B), no signal is attenuated, and the therefore no attenuation is accounted for in the reconstruction. In C), the measured signal is attenuated, however the reconstruction software does not account for this, and the effects are observable. Each panel consists of four angles where the reconstructed image is projected. The number below each reconstruction is the number of panels used, where each panel is linearly spaced angularly, e.g for two panels, the angles [0,90,180,270] consist of one panel, while the second is [45,135,225,315]. The heat map for each is set to be the range between each figures minimum and maximum value.

Figure 4: The mean standard error was calculated for each of the regimes portrayed in Fig.3, with A) consisting of an attenuated signal which is accounted for in the reconstruction, B) including no attenuation characteristics in either signal nor reconstruction, and C) with the attenuation characteristics measured, but not accounted for in the reconstruction process.

used impacted the reconstruction accuracy. The effect of attenuating the light signal, but not accounting for it was also observed, alongside a benchmark reconstruction with no attenuation features.

The Stopping Range of Ions in Matter (SRIM) software was used to ascertain the corresponding spectral resolution for the given thickness of the layer - which is dependent on the number of panels used, the thickness of each fibre, and the fibre material. This modelled CH scintillator fibres from Saint-Gobain [11] as the medium. This is compared to RCF which uses Polyethylene terephthalate.

5 Results

The three regimes explored using the MLEM algorithm are presented in Fig.3 for a different number of panels. Each panel represents a mesh as seen in Fig.2. The regimes include: attenuating the light signal, and accounting for this in the reconstruction, applying no attenuation to the signal, and attenuating the signal but not accounting for this in the reconstruction respectively. The colour bars represent the range in signal amplitude for these regimes.

The MSE and SSIM were calculated for the three regimes and are presented in Fig.4 and

The spectral resolution was calculated using SRIM software for the CH fibres and the base material of RCF, and is represented in Fig.6 as the error bars of the plot. Several permutations of fibre thickness and panel number were presented for comparison.
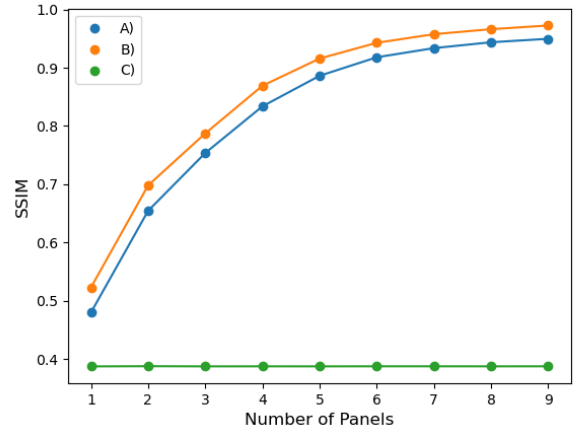
Figure 5: The Structural Similarity Index Matrix was calculated between the original image, and the reconstructed image for a varying number of panels. This was done for both A) attenuated light signal, with the attenuation mechanism incorporated within the reconstruction, B) non-attenuated light signal, and C) attenuated light signal without incorporation of this in the reconstruction. The panels were linearly spaced angularly.

3
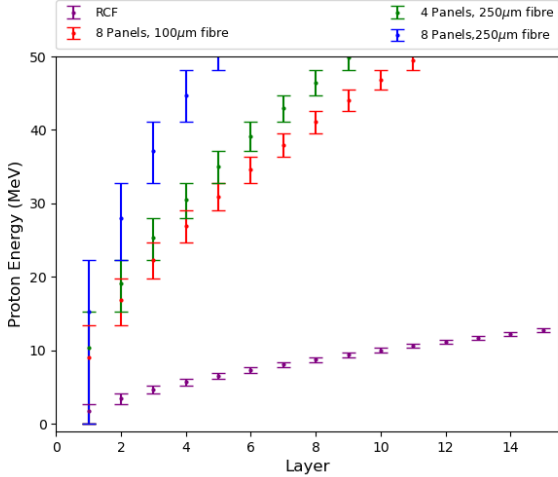
Figure 6: The proton energy deposition simulated with SRIM software package at each layer for one of four conditions labelled above the plot, varying the number of panels, and the thickness of the fibre. The error bars represent the spectral resolution of each condition for the proton energies.

6 Discussion

If disregarded in the reconstruction process the light attenuation significantly affects the reconstruction process, as seen in Fig.3, and quantitatively in Fig.4. The MSE appears constant due to the magnitudinal difference in light signal, as shown in the colour bars of Fig.3. If, however the attenuation is accounted for, the accuracy is of a similar grade to the non-attenuated regime. The MSE suggests that the attenuated form is slightly better to that of the non-attenuated between four to six panels. The reasoning for this is unclear, however, there is a streaking component that is observable for the non-attenuated images within the phantom, that are not present in the attenuated reconstructions in Fig.3. If reconstructions of other images were made, its possible that the performance of the attenuation/no attenuation would be unique to each image. The SRIM (Stopping Range of Ions in Matter) software was used to calculate the depth of peak deposition (Bragg Peak) by the protons for a range of 10keV-10MeV, using the square plastic scintillator fibre properties from Saint-Gobain [11], but for a width of 0.1mm - which is not currently available from the manufacturer, but is intended to be used. The effect on the spectral resolution for a differing number of panels per layer can be seen in Fig.6, where the 2-6 panels' spectral resolution were compared to that of RCF. RCF's spectral measurements were carried out using it's base constituent element; polyester. This compound was Polyethylene terephthalate [12]. RCF also contains another layer called the emulsion layer. SRIM does not allow for simulating ion interactions within non-homogeneous mediums, and so this emulsion layer was disregarded due to having a marginal volume within the film compared to the Polyester [13].

As the number of panels used per layer increases, a higher spatial resolution is attainable if the same image is projected onto all panels. However this corresponds to a lower spectral resolution. It's evident that the spectral resolution of RCF cannot be achieved with these parameters. Thinner fibres would close the gap between the two spectral resolutions, however, with very small fibres diffraction phenomena may become more apparent as the width is now tending towards the wavelength of the light being transmitted.

The figure of merit of tomographic reconstruction often used is the MSE, however many reports include the use of the Structural Similarity Index Matrix (SSIM) which compares the luminance, contrast and structure of the image. A concise explanation of the differences between MSE and SSIM can be found in Ref.[14], where its demonstrated that MSE is not ideal when compared to our own perception of the "likeness" of two images. In particular its shown that spatially shifting an image and comparing significantly increases the MSE, compared to compressed, or blurred versions of the image where the MSE is smaller (but to our perception, more unlike the original). The SSIM was calculated for each reconstruction also, and found that the non-attenuated reconstruction outperformed the attenuated reconstruction for every simulation, as shown in Fig.5. Each pixel value contributes to several readouts from the fibre at non-cardinal angles, and therefore a "smoothing" function is applied to the readout - meaning that sharp contrasts in the original image will take more projected angles to reconstruct accurately. As mentioned, contrast is an important weighting component for the SSIM. A deeper look into the spectral-spatial distributions would be of interest in proving that the smoothing function that occurs in this simulation does not detrimentally impact the reconstruction, and may also be used as a guide in deciding what benchmark is most useful for this simulation.

The choice of the prior image (i.e. the first guess) has been shown to be influential to the reconstruction accuracy [8] [7], however the image used as the initial guess needs to be chosen wisely in order to achieve optimal reconstruction. If MLEM is used as the method to reconstruct, it is suggested that a database be constructed that is capable of sorting through the digitised spectral-spatial distributions based on the energy output of the target, and the expected divergence, among other necessary parameters. A neural network has been applied before to tune the weighting of its reconstruction method according to prior knowledge [15]. The Shepp-Logan phantom was chosen due to its high contrast, and spherical shape, and that if the method was able to reliably reconstruct an image, then it would be able to measure intricate proton emission such as filamention [16] and beam divergence [17].

7   Conclusion

The iterative reconstruction software was successful in reconstructing images, and correctly handling attenuated light signals in order to reconstruct, with the corresponding spectral resolution also described in the Discussion. As the number of projected angles increased, the quality of the reconstruction improved through the mean standard error and the SSIM. However a better benchmark needs to be validated for the reconstruction method proposed. Thinner fibres were shown to improve the spectral resolution at a given number of angles projected, and is therefore the most obvious route to a highly resolved spectral spatial detector.

References

[1] C Brenner et. al. Laser-driven x-ray and neutron source development for industrial applications of plasma accelerators. *Plasma Physics and Controlled Fusion*, 58(014039), 2016.

[2] F Nürnberg et. al. Radiochromic film imaging spectroscopy of laser-accelerated proton beams. *Rev. Sci. Instrum.*, 80(033301), 2009.

[3] J Green et. al. Scintillator-based ion beam profiler for diagnosing laser-accelerated ion beams. *Proc. SPIE*, 8079(807919), 2011.

[4] M Hauault et. al. A 2d scintillator-based proton detector for high repetition rate experiments. *High Power Laser Science and Engineering*, 7, 2019.

[5] D R Rusby et. al. Novel scintillator-based x-ray spectrometer for use on high repetition laser plasma interaction experiments. *Rev. Sci. Instrum.*, 89(073502), 2018.

[6] A.P Dempster et. al. Maximum likelihood from incomplete data via the em algorithm. *Journal of the Royal Statistical Society, Series B*, 39(1), 1977.

[7] T Yu and W Cai. Benchmark evaluation of inversion algorithms for tomographic absorption spectroscopy. *Applied Optics*, 56(8), 2017.

[8] Dan Ma et. al. The performance of MLEM for dynamic imaging from simulated few-view, multi-pinhole SPECT. *IEEE Transactions in Nuclear Science*, 60(1), 2013.

[9] L A Shepp & B F Logan. The fourier reconstruction of a head section. *IEEE Transactions on Nuclear Science*, 21(3), 1974.

[10] H M Gach et. al. 2d 3d shepp-logan phantom standards for mri. *19th International Conference on Systems Engineering*, 2008.

[11] Saint-Gobain. Plastic scintillating fibres. `https://www.crystals.saint-gobain.com/sites/imdf.crystals.com/files/documents/fiber-product-sheet.pdf`. Accessed 01/07/21.

[12] W L McLaughlin et. al. Radiochromic plastic films for accurate measurement of radiation absorbed dose and dose distributions. *Radiaton Physics and Chemistry*, 10:119–127, 1977.

[13] International Specialty Products. Gafchromic® md-v2-55 radiochromic dosimetry film for high-energy photons. `http://www.elimpex.com/new/products/radiation_therapy/Gafchromic/content/GAFCHROMIC\%20MD-V2-55.pdf`. Accessed 20/07/21.

[14] Z Wang and A C Bovik. Mean squared error: Love it or leave it. *IEEE Signal Processing Magazine*, 98, 2009.

[15] D Micielli. Accelerating neutron tomography experiments through artificial neural network based reconstruction. *Scientific Reports*, 9(2450), 2019.

[16] M Quinn et. al. On the on the investigation of fast electron beam filamentation in laser-irradiated solid targets using multi-mev proton emission. *Plasma Physics and Controlled Fusion*, 53(124012), 2011.

[17] B Albertazzi et. al. A compact broadband ion beam focusing device based on laser-driven mega-gauss thermoelectric magnetic fields. *Rev. Sci. Instrum.*, 86(043502), 2015.